Materials Today Physics 48 (2024) 101549

Contents lists available at ScienceDirect

Materials Today Physics

journal homepage: www.journals.elsevier.com/materials-today-physics

An interpretable formula for lattice thermal conductivity of crystals

Xiaoying Wang [a], Guoyu Shu [a], Guimei Zhu [b], Jian-Sheng Wang [c], Jun Sun [a], Xiangdong Ding [a], Baowen Li [d,**], Zhibin Gao [a,*]

[a] State Key Laboratory for Mechanical Behavior of Materials, School of Materials Science and Engineering, Xi'an Jiaotong University, Xi'an, 710049, China
[b] School of Microelectronics, Southern University of Science and Technology, Shenzhen, 518055, China
[c] Department of Physics, National University of Singapore, Singapore, 117551, Republic of Singapore
[d] Department of Physics, Department of Materials Science and Engineering, Southern University of Science and Technology, Shenzhen 518055, PR China

A B S T R A C T

Lattice thermal conductivity (κ_L) is a crucial physical property of crystals with applications in thermal management, such as heat dissipation, insulation, and thermoelectric energy conversion. However, accurately and rapidly determining κ_L poses a considerable challenge. In this study, we introduce a formula that achieves high precision (mean relative error = 8.97 %) and provides fast predictions, taking less than 1 min, for κ_L across a wide range of inorganic binary and ternary materials. Our interpretable, dimensionally aligned and physical grounded formula forecasts κ_L values for 4601 binary and 6995 ternary materials in the Materials Project database. Notably, we predict undiscovered high κ_L values for $AlBN_2$ ($\kappa_L = 101$ W m^{-1} K^{-1}) and the undetected low κ_L Cs_2Se ($\kappa_L = 0.98$ W m^{-1} K^{-1}) at room temperature. This method for determining κ_L streamlines the traditionally time-consuming process associated with complex phonon physics. It provides insights into microscopic heat transport and facilitates the design and screening of materials with targeted and extreme κ_L values through the application of phonon engineering. Our findings offer opportunities for controlling and optimizing macroscopic transport properties of materials by engineering their bulk modulus, shear modulus, and Grüneisen parameter.

1. Introduction

Materials with ultrahigh or low thermal conductivity (κ_L) are desirable for many technological applications. In the realm of heat dissipation and on-chip cooling, the main challenges for the future development of microelectronics, driven by Moore's law, include several key issues [1–4]. Also GaN-based power devices is calling for high κ_L [5,6]. Another aspect, thermal insulation and thermoelectric technology which enables the direct conversion between heat and electricity requires low κ_L. The conversion efficiency is determined by the dimensionless figure of merit (ZT), which is defined as $ZT = S^2\sigma/(\kappa_e + \kappa_L)$ (where σ, S, T and κ_e represent the electrical conductivity, Seebeck coefficient, absolute temperature and electronic thermal conductivity, respectively). Since the conflicting electronic transport properties [7,8], pushing low κ_L to the limit of best thermal insulators [9] is a favorable strategy to gain high ZT materials [10].

So far, there are many traditional approaches to obtain κ_L of inorganic semiconductor materials. On the theoretical aspect, one can use (i) phonon Boltzmann transport equation (BTE) with *ab initio* study [11], (ii) molecular dynamics simulations with Green-Kubo or Fourier's law [12], (iii) nonequilibrium Green's function [13], and (iv) scattering-matrix [14]. For the experiment, there are (i') micro-fabricated suspended thermal bridge [15,16], (ii') micro-Raman spectroscopy [17], (iii') 3ω method [18], and (iv') time-domain thermoreflectance (TDTR) [19].

Nevertheless, the theoretical calculation is usually limited by insufficient accuracy, time-consuming, and the appropriate interatomic force constants (IFCs). The experimental one is always highly dependent on leading-edge instruments and the quality of the sample [20,21]. To overcome above inherent disadvantages, empirical model and other newly-developed formula based on machine learning (ML) provide new insights[22–27].

It is reported that the strategy of formula based on empirical and newly-developed technique have made great progress. Empirical methods raised several analytical models for lattice thermal conductivity including the widely-known Slack model [22] and Debye–Callaway Model [28]. Furthermore, machine learning (ML) methods have been supplied to obtain the formula for the prediction of thermal conductivity in recently several studies[29–31].

However, a difficult-to-obtain directly parameter in the formula, such as Debye temperature θ, hinders the ability to screen and predict thermal conductivity rapidly. Furthermore, Machine learning formulas

* Corresponding author.
** Corresponding author.
E-mail addresses: libw@sustech.edu.cn (B. Li), zhibin.gao@xjtu.edu.cn (Z. Gao).

https://doi.org/10.1016/j.mtphys.2024.101549
Received 28 June 2024; Received in revised form 16 August 2024; Accepted 5 September 2024
Available online 7 September 2024

tend to have complex forms and large amount of parameters, which pose a common drawback is that most of these models consider physical dimensional alignment. Existing a complex formula and an ambiguous physical interpretation [32,33]. Moreover, more and more investigation testified that calculating the thermal conductivity requires consideration of higher order scattering, we put high-order scattering factor δ into considering.

In this work, we first collect all available κ_L materials from the AFLOW database [34]. Then we detect some key physical quantities as a function of κ_L aided by Pearson correlation analysis (Fig. 2). We further relate these parameters to elastic mechanics, phonon-phonon scattering, relaxation time approximation, and domain knowledge, simplifying the Slack formula with a more precise and compact form written as Eq. (13). Comparison of the formula's calculation results with AFLOW database, Slack formula and density functional theory (DFT) are conducted in order to confirm its accuracy. For the application of formula, considering the "small data" characteristics of Grüneisen parameter γ, we solve it through crystal graph convolutional neural networks (CGCNN) as illustrated in Fig. 5(c). Finally we apply our formula for predicting thermoelectric materials. The overview of entire process is provided in Fig. 1.

Our proposal has a universal and simple empirical formula with strong generalization ability and clear physical meaning. Our formula, Eq. (13), coupled with the machine learning method, is not only accurate but also able to predict κ_L rapidly. Especially used in low thermal conductivity materials attributed to the limited amount of high thermal conductivity gamma data causes CGCN to predict gamma accuracy less accurately than low thermal conductivity gamma data. We finally apply our method to 4601 binary and 6995 ternary inorganic compounds in the Materials Project database, which can accelerate the materials discovery process with targeted κ_L and reduce the design and screening costs in thermal management, on-chip cooling, and thermoelectrics.

2. A surrogate formula for lattice thermal conductivity

In this section, we derive our key finding of a more concise and accurate formula for predicting thermal conductivity, Eq. (13), from analysis of Pearson correlation coefficients (PCC) and some physics arguments.

Due to a large number of parameters affecting κ_L, we initially use the PCC which is defined in Supplemental Material, to select critical parameters and proper descriptors [35]. Fig. 2(a) displays the correlogram for whole inorganic compounds crystals from AFLOW database [34] between the following variables: lattice thermal conductivity κ_L, electronic band gap, speed of sound υ_s, Poisson's ratio ν, bulk modulus B, shear modulus G, Young's modulus E, Debye temperature $\theta_{D,a}$, Grüneisen parameter γ, heat capacity C_V, lattice constant a, their atomic radius r_a, r_b, their atomic mass m_a, m_b, their electron affinity E_{ea}, E_{eb}, their ground state energy per atoms E_{a0}, E_{b0}, their number of valence electrons VE_a, VE_b, their electronegativities χ_a, χ_b, and their atomic number Z_a, Z_b.

It is interesting to note that G, E, C_V, $\theta_{D,a}$, υ_s, and B are largely correlated with thermal conductivity κ_L, shown in Fig. 2(b). The correlation value between these parameters and κ_L is almost more than 70 % by PCC analysis. G, E, B and υ_s are the physical quantities of elastic mechanics, while C_V and $\theta_{D,a}$ are parameters of thermodynamics. For the Peierls-Boltzmann transport equation, the lattice thermal conductivity κ_L can be calculated as

$$\kappa_{\alpha\beta} = \frac{1}{V}\sum_{\lambda} C_\lambda \upsilon_{\lambda\alpha}\upsilon_{\lambda\beta}\tau_\lambda, \tag{1}$$

where V is the crystal volume, λ denotes a phonon mode with a different wave vector and branch index. α and β denotes the Cartesian directions. C_λ is the specific heat per mode, $\upsilon_{\lambda\alpha}$ and τ_λ are the velocity component along α direction and the relaxation time of the phonon mode λ.

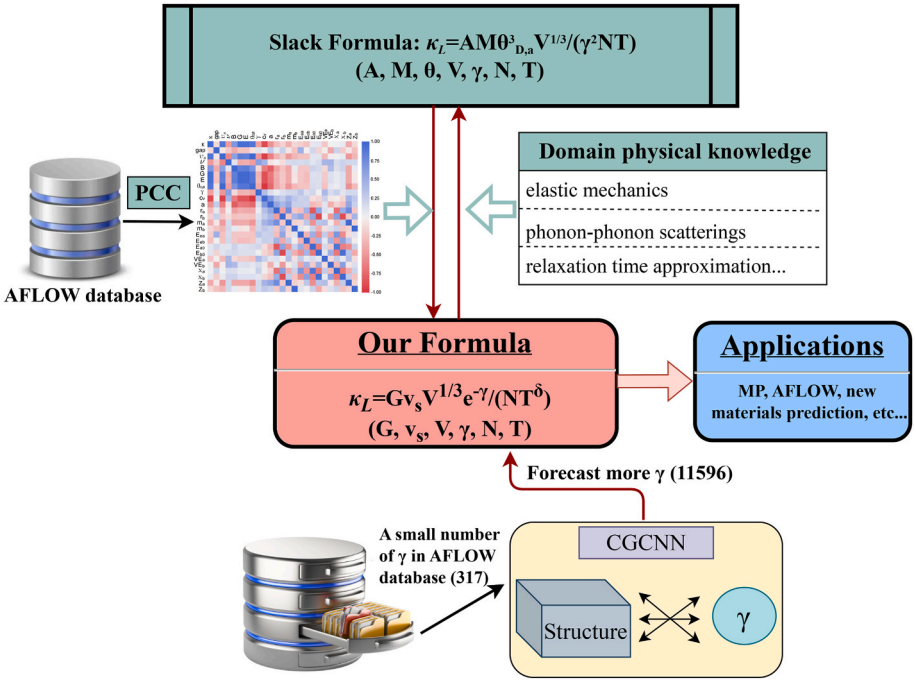

Fig. 1. The schematic framework of the proposed approach. In the Slack model, M is the atomic mass of the atom and V is the volume of the primitive cell. $\theta_{D,a}$ is the Debye temperature of acoustic phonons. γ, N, and T are Grüneisen parameters, the number of atoms in the primitive cell, and absolute temperature, respectively. The added parameters G and υ_s in our formula represent the shear modulus and the phonon velocity of sound, respectively. In the process of formula derivation, υ_s can be replaced by ρ, B (Bulk modulus) and G according to Eq. (5). We screened a total 317 number of γ data from the ALFOW database and predicted a total of 11596 γ data through crystal graph convolutional neural network (CGCNN). We used Pearson correlation coefficients (PCC) to analyze correlated parameters and via domain knowledge, derive an interpretable formula. We finally apply our method to all binary and ternary inorganic compounds in the Materials Project and AFLOW database, which can accelerate the materials discovery process with targeted κ_L.

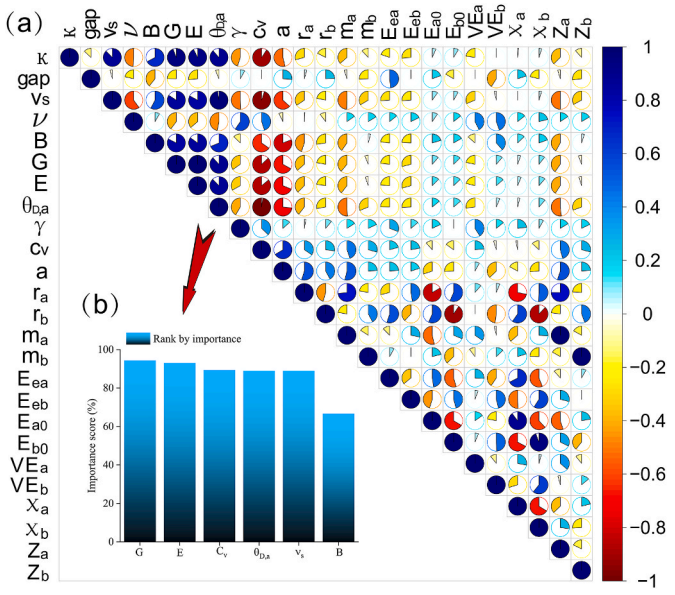

Fig. 2. (a) Pearson correlation coefficient (PCC) between lattice thermal conductivity κ_L, electronic band gap, speed of sound υ_s, Poisson's ratio ν, bulk modulus B, shear modulus G, Young's modulus E, Debye temperature $\theta_{D,a}$, Grüneisen parameter γ, heat capacity C_V, lattice constant a, their atomic radius r_a, r_b, their atomic mass m_a, m_b, their electron affinity E_{ea}, E_{eb}, their ground state energy per atoms E_{a0}, E_{b0}, their number of valence electrons VE_a, VE_b, their electronegativities χ_a, χ_b, their atomic number of atoms Z_a, Z_b for inorganic compounds crystals. The blue section is a positive correlation, while the red one is a negative correlation. (b) The importance ranking of features via the PCC method is shown at the left bottom. (For interpretation of the references to color in this figure legend, the reader is referred to the Web version of this article.)

Therefore, κ_L is a coupling effect between harmonic IFCs and higher-order ($\geq$3) IFCs [36]. Note that PCC is a linear correlation analysis but κ_L, especially phonon relaxation time τ, originates from the higher-order phonon-phonon scattering [37]. Therefore, we should clarify the relationship between these physical quantities. Besides, the Grüneisen parameter γ has been shown to significantly affect the value of thermal expansion and κ_L [38], even if its PCC value is less than 50 % shown in Fig. 2(a). Therefore, based on the PCC analysis and domain knowledge, G, E, B, υ_s (harmonic effect), C_V, $\theta_{D,a}$, and γ (anharmonic effect) are selected as the most critical feature descriptors for κ_L.

Various early estimates of κ_L of a solid at temperatures not too far removed from the Debye temperature has been discussed by Slack [22]. This estimate takes the form,

$$\kappa_L = A\frac{M\theta_{D,a}^3 V^{\frac{1}{3}}}{\gamma^2 NT}, \tag{2}$$

where M is the atomic mass of the atom and V is the volume of the primitive cell. $\theta_{D,a}$ is the Debye temperature of acoustic phonons. γ, N, and T are Grüneisen parameters, the number of atoms in the primitive cell, and absolute temperature, respectively. There are two kinds of expression of the parameter A, one is $A(\gamma) = \frac{2.43\times10^{-8}}{(1-\frac{0.514}{\gamma}+\frac{0.228}{\gamma^2})\gamma^2}$ given by Julian [39], and other one is $A = 3.04\times10^{-8}$ obtained by Slack [22]. Since γ in most materials can not reach 2 and is a variable quantity rather than a constant number, we use a proportional expression that is dimensionally aligned,

$$\kappa_L \propto \frac{M\theta_{D,a}^3 V^{\frac{1}{3}}}{NT}. \tag{3}$$

Combing the traditional definition for Debye temperature $\theta_D = \frac{\hbar\upsilon_s}{k_B}(\frac{3}{4\pi}\frac{N}{V})^{\frac{1}{3}}$ and derived directly from the phonon density of states by integrating only over the acoustic modes $\theta_{D,a} = \theta_D/N^{\frac{1}{3}}$ [40], then $\theta_{D,a}$ can be expressed as Eq. (4)

$$\theta_{D,a} = \frac{h}{k_B}\left(\frac{3}{4\pi}\frac{1}{V}\right)^{\frac{1}{3}}\upsilon_s, \tag{4}$$

Basically, υ_s is the speed of sound in the elastic mechanics and can be calculated by the transverse velocity υ_t and the longitudinal velocity υ_l [41],

$$\begin{aligned}\upsilon_s &= \left\{\frac{1}{3}\left[\frac{1}{\upsilon_l^3}+\frac{2}{\upsilon_t^3}\right]\right\}^{-\frac{1}{3}}\\ \upsilon_l &= \sqrt{\frac{B+\frac{4}{3}G}{\rho}}\\ \upsilon_t &= \sqrt{\frac{G}{\rho}},\end{aligned} \tag{5}$$

Inserting Eq. (4) into Eq. (3), the lattice thermal conductivity can be transformed into a new form,

$$\kappa_L \propto \frac{3h^3}{4\pi k_B^3}\cdot\frac{M}{V}\cdot\frac{V^{\frac{1}{3}}\upsilon_s^3}{NT}, \tag{6}$$

One can remove the constant terms and attain,

$$\kappa_L \propto (\rho\upsilon_s^2)\left(\frac{\upsilon_s V^{\frac{1}{3}}}{NT}\right), \tag{7}$$

where ρ is the density of a material. κ_L is proportional to the hardness as expressed in the preceding study, a single crystal diamond has a 4100 W m^{-1} K^{-1} at 104 K [42]. Besides, carbon nanotube [43] and silicon carbide [44] are also good cases. Consequently, it is assumed that κ_L is proportional to the (Vickers) hardness of materials. $\kappa_L \propto H_V$, it is intuitive to assume that they deliver similar information about κ_L. Therefore, one can use hardness H_V to replace $\rho\upsilon_s^2$,

$$\kappa_L \propto H_V\cdot\left(\frac{\upsilon_s V^{\frac{1}{3}}}{NT}\right). \tag{8}$$

A renowned work [45] found that H_V is rigorously proportional to shear modulus G, rather than Young's modulus E. Thus, neglecting the contribution of plasticity [46], hardness H_V can be precisely estimated by Ref. [45],

$$H_V = 0.151\cdot G, \tag{9}$$

and κ_L can be expressed as,

$$\kappa_L \propto \frac{G\upsilon_s V^{\frac{1}{3}}}{NT}\cdot B(\gamma), \tag{10}$$

where $B(\gamma)$ is a dimensionless term associated with Grüneisen parameter γ. A question arises naturally: what is the relationship between B(γ) and phonon relaxation time? According to the work of Klemens, the inverse relaxation time of phonons for U-type process can be written as [47],

$$\tau_U^{-1} = B_U\omega T^3\cdot\exp\left(-\frac{\theta_D}{\alpha T}\right), \tag{11}$$

where phonon relaxation time τ and Debye temperature e^{θ_D} is a positive correlation. Besides, $\theta_D = \omega_{\max}/k_B$ and $\gamma = -d\ln\omega/d\ln V$, combing Eq. (11), one can conclude that τ is negatively proportional to γ. Moreover, they are likely to have an exponential relationship. Based on the above

theoretical derivation and domain knowledge [47], we propose that $B(\gamma) = e^{-\gamma}$ and the final thermal conductivity is,

$$\kappa_L = \frac{G\upsilon_s V^{\frac{1}{3}}}{NT} \cdot e^{-\gamma}, \tag{12}$$

Note that Eq. (12), in consistent with the Slack model of Eq. (2), only consider the contribution from acoustic phonon branches, which is good for common materials, in which group velocities of optical branches are small and the acoustic branch dominates the heat transport. Therefore, for other materials wherein the optical branches play a critical role, the formula needs to be revised, for example, BaO whose κ_L is estimated of 14.15 W m^{-1} K^{-1} [48], while the experimental value is 2.3 W m^{-1} K^{-1} [48]. We revise the rate of κ_L decline by,

$$\kappa_L = \frac{G\upsilon_s V^{\frac{1}{3}}}{NT^{\delta}} \cdot e^{-\gamma}. \tag{13}$$

where δ is somewhere between 1 and 2. The precise theory of the power law is quite complex, having to do with competition between scattering processes produced by cubic and quartic anharmonic terms [37,49]. In the following, we only consider three-phonon scattering with $\delta = 1$. Therefore, combining the PCC analysis and physical domain knowledge, we derive an interpretable and dimensionally aligned formula for lattice thermal conductivity.

Our formula, Eq. (13) has several advantages compared to the Slack model, Eq. (2): (i) The Debye temperature (θ_D) is replaced by the Shear modulus (G) and sound velocity (υ_s). These two parameters are more conveniently obtained and searchable from databases such as the Materials Project and AFLOW. (ii) The exponential form of our Grüneisen parameter (γ) incorporates Kelemens's well-known relaxation time approximation for U-type phonon-phonon scattering processes in Eq. (11), compared with the experimental fit of γ^2 in the Slack model. (iii) Our formula can incorporate fourth-order phonon scattering using the T^{δ} form, where δ is somewhere between 1 and 2.

3. Formula validation with the slack model

In order to verify the accuracy of our formula with AFLOW database (currently there is no such high accuracy LTC database available, and using AFLOW medium accuracy LTC data might be the best choice), we collect the whole ALFOW compounds which was calculated by the formula as [40],

$$\kappa(T) = \frac{0.849 \times 3 \times 4^{\frac{1}{3}}}{20\pi^3 \left(1 - 0.514\gamma_a^{-1} + 0.228\gamma_a^{-2}\right)} \cdot \left(\frac{\kappa_B \theta_a}{\hbar}\right)^2 \cdot \frac{\kappa_B m V^{\frac{1}{3}}}{\hbar \gamma_a^2} \frac{\theta_a}{T} \tag{14}$$

For comparison, we also find an obvious linear relationship between the thermal conductivity of the slack model and the AFLOW database, as shown in Supplemental Information Fig. S2. Consequently, we can directly compare the results of our formula and slack model with AFLOW database to demonstrate and validate their accuracy.

Downloadable databases of κ_L include 4363 single, binary, and ternary inorganic materials. The result is shown in Fig. 3. The horizontal axis represents predicted κ_L based on Eq. (12) and the vertical axis plots the κ_L originating in the AFLOW database [34]. The black data points are essentially concentrated on the range of the $y = x$ function, indicating a high degree of proximity for our formula. We also list 42 familiar materials from four crystal systems to verify Eq. (12), coupled with the experimental data shown in the Supplemental Material. The data distribution is shown in the inset marked with the number of space groups.

Meanwhile, our formula can also be used for different crystal systems, as shown in Fig. 3 with different symbols and colors. The error analysis displays that the majority of materials are surrounded within 100 % in gray color. We also plot the corresponding experimental measurement. It should be pointed out that the data are distributed in various space groups as shown in inset, illustrating that our formula has

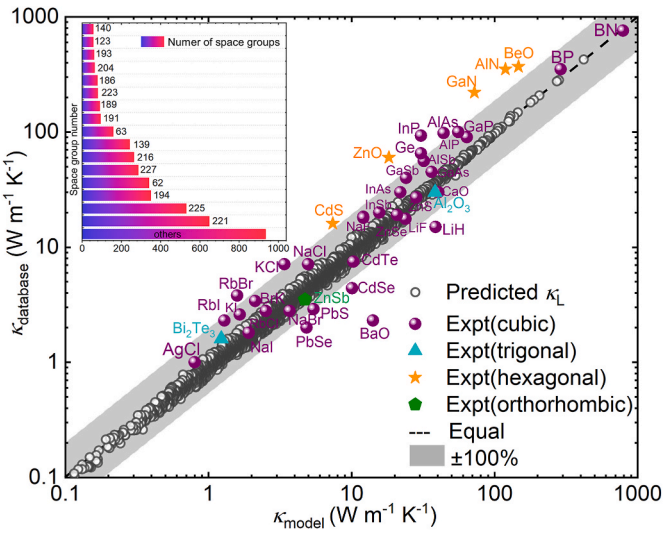

Fig. 3. Comparison of thermal conductivity κ_L at 300 K between our formula prediction and ALFOW database [34] with gray hollow points. The purple, cyan, orange, and green colors stand for experimental measurement (AgCl [50], Al_2O_3 [51], BaO [48], ZnSb [52], Bi_2Te_3, CdSe [53], AlAs, AlN, AlP, AlSb, BeO, BN, BP, CaO, CdS, CdTe, GaAs, GaN, GaP, GaSb, Ge, InAs, InP, InSb, KBr, KCl, KI, LiH, LiF, NaBr, NaCl, NaF, NaI, PbS, PbSe, PbBr, RbCl, RbI, ZnO, ZnS, ZnSe, and ZnTe [38]) with cubic, trigonal, hexagonal, and orthorhombic crystal systems, respectively. The dashed black line is the function of $y = x$. The inset in the upper left corner represents the distribution of the number of space groups (the horizontal axis) for all materials. The vertical axis represents the index of the space group. (For interpretation of the references to color in this figure legend, the reader is referred to the Web version of this article.)

an effective prediction for various crystal structures and element independence. It is noteworthy from Fig. 3 that our model achieves a high accuracy of our proposed framework and provides a novel methodology for designing unusual materials with targeted properties, such as ultrahigh and ultralow κ_L. Besides, the whole computational cost, compared to the *ab initio* study, is almost negligible.

Besides, we not only can predict the AFLOW database but also apply it to other new materials. Here, we adopt the precursor Materials Project to make a prediction. We estimate γ and κ_L based on our model for 4601 binary and 6995 ternary inorganic materials from the Materials Project. All results are shown in the Supplemental Material MP-binary and MP-ternary. Part of their κ_L was not published to the best of our knowledge. Therefore, our model can be a good predictor to compare, rank, and design the unknown materials.

4. Accuracy comparison between our formula and DFT study

Combining our empirical model of high-throughput computation for predicting κ_L, we demonstrate the empirical formula as a function of the Shear modulus predicted by our model (Fig. 4(a)). Mapping relation exists in G with κ_L visibly. It is proved that G plays a significant role in thermal conductivity and our model is truthful.

Afterwards, in order to verify the accuracy of our model compared with the theoretical calculation, we employed *ab initio* density functional theory (DFT) calculation by randomly selecting two kinds of high κ_L materials (blue dotted lines) and two kinds of low κ_L materials (red dotted lines), shown in Fig. 4(b). The physical parameters output from the selected materials are shown in Table 1. More computation details are putting into Supplemental Material.

In Fig. 4(b) and Table 1, the Grüneisen parameter γ of SiC is 0.66 at 300 K. Coupled with G (187 GPa) and B (211 GPa), one can obtain κ_{model} of 369.53 W m^{-1} K^{-1} based on our model. Well match with solving the phonon BTE by DFT calculation, SiC has a value of 420.65 W m^{-1} K^{-1} at room temperature. Similarly, for also high κ material, $AlBN_2$ has a γ of

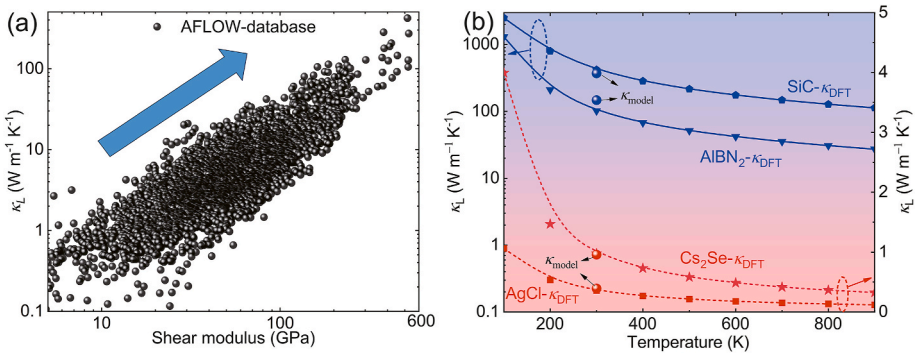

Fig. 4. (a) The relationship of Shear modulus G and κ_L originated from the AFLOW database. (b) Example of ultrahigh and ultralow thermal conductivity κ_L materials between our formula predictions (solid symbols) and *ab initio* calculations (solid and dashed lines). The Grüneisen parameter γ of 300 K was substituted into our formula to obtain κ_L represented as bullets.

Table 1
Eleven examples of materials from the Materials Project database. ρ (g·cm^{-3}), V (Å^3), G (GPa), B (GPa), and N represent density, volume, Shear modulus, Bulk modulus, and number of atoms in the primitive cell, respectively. κ_{DFT} and κ_{model} (W m^{-1} K^{-1}) stand for lattice thermal conductivity from the ShengBTE code and our proposed model from Eq. (13). Except for $AlBN_2$ and Cs_2Se are novel materials that have never been reported about their κ_L, we also display some experimental results, SiC [54], AgCl [50], $CsPbBr_3$ [37], CdS [38], MgO [38], GaN [38], LiH [55], RbBr [38], RbI [38], comparing them with our first principles calculations and the results of our formula.

Materials	ID-number	ρ	V	G	B	N	Symmetry	κ_{exp}	κ_{DFT}	κ_{model}
Cs_2Se	mp-1011695	3.73	153.89	5	12	3	Cubic	/	0.98	0.96
$AlBN_2$	mp-1008557	3.33	32.82	177	258	4	Cubic	/	101.54	146.81
SiC	mp-8062	3.17	21.00	187	211	2	Cubic	490	420.65	369.53
AgCl	mp-22922	5.58	44.43	7	43	2	Cubic	1	0.36	0.39
$CsPbBr_3$	mp-567681	5.01	769.21	6	12	20	Orthorhombic	0.35	0.32	0.18
CdS	mp-672	4.58	104.86	18	53	4	Cubic	16	12.53	7.41
MgO	mp-1265	3.47	19.28	119	151	2	Cubic	60	68.4	80.74
GaN	mp-804	5.92	46.94	105	172	4	Cubic	220	266.4	321.82
LiH	mp-23703	0.82	16.00	43	37	2	Cubic	18.3	19.7	25.49
RbBr	mp-22867	3.16	86.78	6	14	2	Cubic	3.8	4.97	1.59
RbI	mp-22903	3.36	104.96	5	10	2	Cubic	2.3	1.74	1.29

0.94. By substituting γ into Eq. (13), we can get a κ_{model} is 146.81 W m^{-1} K^{-1} at 300 K, while the *ab initio* study is 101.54 W m^{-1} K^{-1}. The result shows that our model has a small error compared with the DFT calculation for high thermal conductivity materials. On the other hand, for the low thermal conductivity materials, γ of Cs_2Se and AgCl are 1.41 and 2.61 and the predicted κ_{model} are 0.96 W m^{-1} K^{-1} and 0.39 W m^{-1} K^{-1} at 300 K, respectively. For the phonon BTE calculation, κ_{DFT} are 0.98 W m^{-1} K^{-1} and 0.36 W m^{-1} K^{-1} of both materials.

In this sense, our model is more accurate for low thermal conductivity materials than high κ_L materials. But all prediction results and DFT results are of the same order of magnitude, which implies our model can be used for screening and designing targeted κ_L materials with tunable density, volume, Bulk modulus, and number of atoms in the primitive cell by phonon engineering [56].

5. Machine learning aids formula parameter γ

In brief, in order to acquire the thermal conductivity κ_L, except for the crystal structure acquiring volume of the primitive cell and the number of atoms, there are only three parameters that need to be known: B (so as to obtain υ_s according to Eq. (5)), G, and γ. γ can normally be estimated by the thermal expansion data. The calculation of γ needs high computational cost [36], using the trained CGCNN method is a fast and efficient method of obtaining large quantities of γ [57]. B and G are elastic results but γ are inelastic response. Therefore, linear response parameters B and G are easier to obtain than γ which is nonlinear.

In order to provide more support for conducting thermal conductivity calculations based on B and G data. We use the CGCNN method to predict the B and G, shown in Fig. 5(a) and (b). Furthermore, we obtained all existing γ values of binary and ternary compounds from the AFLOW database [34] and used them as a training process to build a nonlinear mapping network between the crystal structure and phonon anharmonicity γ as shown in Fig. 5(c).

R^2 (root mean square error) evaluates the accuracy of γ between the predicted values and benchmark from the AFLOW database. R^2 for B, G, and γ are 0.920, 0.915, and 0.869, respectively. The model performance of γ is comparatively trustworthy and can be used for subsequent κ_L prediction based on Eq. (13). We supply predicted γ into our formula associating with existing renowned database Material Project, totally 4601 binary and 6995 ternary novel materials. As displayed in Supplemental Material (MP-binary and MP-ternary files).

Moreover, due to the limitation of number in high thermal conductivity materials for the Gruneisen parameter, consequently, CGCNN's prediction of some high thermal conductivity materials gamma is not very accurate. There is a lack of correspondence between the partial predicted results and experimental results of partial materials.

6. Prediction of a new thermoelectric material

On account of Low κ_L is a favorable factor to gain high ZT materials and best thermal insulators. In order to expand the application of our formula, we select one unreported low κ_L material, Cs_2Se, as an example, to explore the potential thermoelectric performance.

The phonon and electronic transport properties of Cs_2Se are shown in Fig. 6. Based on quasi-harmonic approximation, we notice that our predicted κ_L agreed with the DFT calculation. However, recent works show that four-phonon scattering and quartic anharmonicity play a critical role in heat transport [37,58,59]. We label this advanced method as abbreviated SCPH+3ph, SCPH+3,4ph. We adopt the rigorous

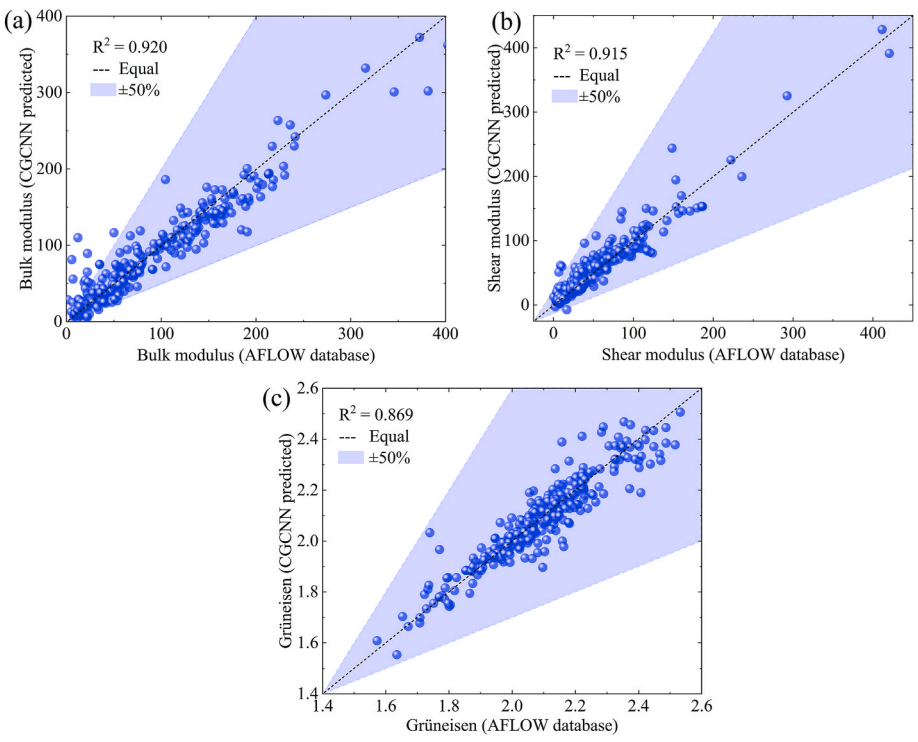

Fig. 5. (a) Based on the CGCNN framework, the correlation of Bulk modulus (B) between our predicted values and the AFLOW database. (b) The correlation of Shear modulus (G) between our predicted values and the AFLOW database. (c) Comparison of γ between our trained-CGCNN prediction and the benchmark of the AFLOW database [34].

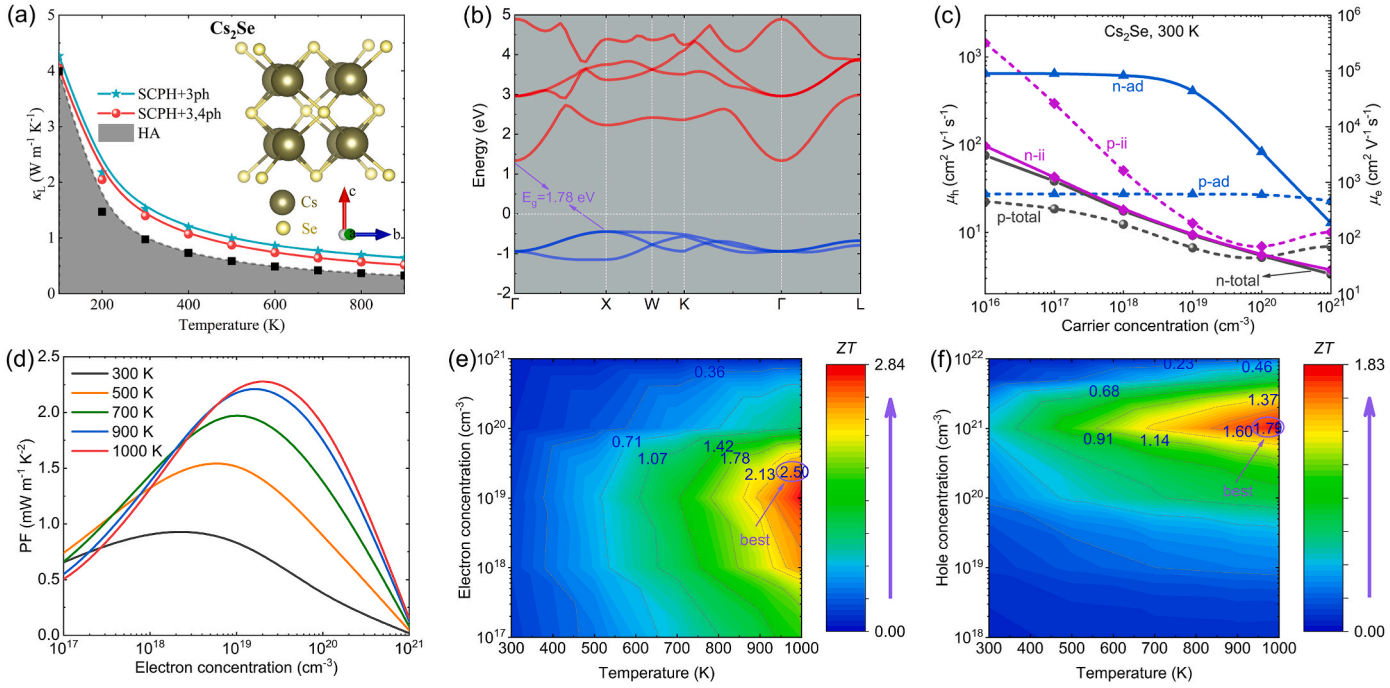

Fig. 6. The calculated transport performance for predicted Cs_2Se novel materials. (a) The computed lattice thermal conductivity of harmonic approximation (HA), third-order anharmonicity phonon renormalization (SCPH+3ph), and quartic anharmonicity phonon renormalization (SCPH+3,4ph) of Cs_2Se as a function of temperature. (b) Electronic band structure with conduction bands (red) and valence bands (blue), respectively. The electronic band gap is 1.78 eV of Cs_2Se. (c) Hole p-type mobility with dotted lines (left ordinate) and electronic n-type mobility with solid lines (right ordinate) as a function of carrier concentration. Scattering mechanisms not only consider the acoustic deformation (ad) potential scattering (blue) but also include ionized impurity (ii) scattering (purple). The total mobility is marked in black solid (n-total) and dashed (p-total) lines as a function of carrier concentration. (d) Power factor $PF = S^2\sigma$ for n-type Cs_2Se electronic transport at 300 K, 500 K, 700 K, 900 K, and 1000 K, respectively. Contour plot of thermoelectric figure of merit ZT for (e) n-type and (f) p-type Cs_2Se as a function of temperature and carrier concentration. The lattice thermal conductivity κ_L is calculated by self-consistent (SCPH) theory and the four-phonon scattering mechanism. (For interpretation of the references to color in this figure legend, the reader is referred to the Web version of this article.)

self-consistent phonon (SCPH) approximation which comprises the first-order contribution to the phonon self-energy and temperature-dependent phonons [58,59]. 3ph represents three-phonon is taken into account. 3,4ph means both three-phonon and four-phonon scattering are considered. More details of Cs_2Se κ_L can be found in Fig. 6(a).

Due to the temperature renormalization and stiffening of phonon dispersion, κ_L (SCPH+3ph) is larger than κ_L (SCPH+3,4ph). Moreover, the quartic anharmonicity induces extra phonon-phonon scattering, leading to a smaller κ_L (SCPH+3,4ph) compared with κ_L (SCPH+3ph).

All energy bands are shifted to the Fermi level at 0 eV shown in Fig. 6 (b). It has an indirect band gap of 1.78 eV. Renowned SnSe is a layered crystal with a band gap of 0.86 eV [10]. Recent work shows that operating at a high temperature is a priority for high band-gap materials [60]. The best thermoelectric performance at the optimal working temperature is restricted by the band gap (E_g) owing to $E_g = 2eS_{\max}T$, where e is the unit charge, $S_{\max}$ is the maximum Seebeck coefficient, and T is the temperature that corresponds to $S_{\max}$. In this sense, wide-band gap semiconductors may work over a wide temperature range and the ZT values are not saturated at high temperatures.

Fig. 6(c) plots the holes (p-type in blue) and electrons (n-type in purple) mobility of Cs_2Se at 300 K. On the basis of electronic BTE, the electronic relaxation time (τ) must be given to obtain the mobility μ and electric conductivity σ. On the one hand, some researchers will approximately adopt a constant relaxation time of 10–12 fs [61]. Therefore, the total mobility is expressed as $1/\tau_{total} = 1/\tau_{ad} + 1/\tau_{ii}$. Both type of mobility decreases as a function of carrier concentration due to the enhanced electron-phonon scattering. n-type total mobility is much higher than p-type at the same carrier concentration.

Because the electric conductivity increases with the carrier concentration, the Seebeck coefficient decreases with the concentration, so there is an optimal doping for the power factor ($PF = S^2\sigma$). The n-type power factor increase as a function of temperature, while the p-type PF is reduces with the temperature increasing as shown in the Supplemental Material Fig. S11. The largest n-type power factor is 2.3 mW m^{-1} K^{-2} for Cs_2Se at 1000 K, shown in Fig. 6(d). The largest p-type power factor is 3.4 mW m^{-1} K^{-2} at 300 K. From Fig. 6(b), the valence band maximum (VBM) is flatter than conduction band minimum (CBM), resulting in a "pudding-mold" which consists of a dispersive portion and a flat portion, can in general be favorable for the coexistence of large Seebeck coefficient and small resistivity [62]. Therefore, p-type Cs_2Se has a larger power factor compared with n-type.

With all of the above results of phonon transport electron transport properties, ZT can be determined, as shown in contour plot Fig. 6(e) and (f). Cs_2Se displays the largest ZT value of 2.50 (1.79) for n-type (p-type) at 1000 K. Such a high ZT value is comparable to the 2.6 ± 0.3 at 923 K in SnSe [10] and other Copper ion liquid-like thermoelectrics [63]. Our calculation suggests that Cs_2Se is a promising material for thermoelectric applications, especially for operating at a high temperature range and also provides a guidance for unveiling new thermoelectric materials based on low κ_L.

7. Conclusions

In summary, building upon the Slack model, we derived an enhanced formula for quickly and conveniently calculating lattice thermal conductivity, incorporating relaxation time approximation and fourth-order phonon scattering. Our findings include: (i) a strong correlation between lattice thermal conductivity, Shear modulus, speed of sound, and Grüneisen parameter; (ii) the development of an interpretable, fast, and accurate theoretical formula for lattice thermal conductivity, Eq. (13), by integrating fundamental physical principles with machine learning; (iii) the potential use of the theoretical formula, Eq. (13), in discovering new materials for heat dissipation, thermoelectrics, and refrigeration, characterized by ultralow or ultrahigh thermal conductivity.

CRediT authorship contribution statement

Xiaoying Wang: Writing – original draft, Software, Methodology, Investigation. **Guoyu Shu:** Software, Resources, Methodology, Investigation. **Guimei Zhu:** Validation, Supervision. **Jian-Sheng Wang:** Validation, Supervision. **Jun Sun:** Validation, Supervision. **Xiangdong Ding:** Validation, Supervision. **Baowen Li:** Validation, Supervision. **Zhibin Gao:** Supervision, Software, Data curation.

Declaration of competing interest

The authors declare that they have no known competing financial interests or personal relationships that could have appeared to influence the work reported in this paper.

Data availability

There is no restriction on sharing the data presented in the text

Acknowledgements

We acknowledge the support from the National Natural Science Foundation of China (No.52250191 and No.12104356). This work is supported by the Key Research and Development Program of the Ministry of Science and Technology under Grant No.2023YFB4604100. We also acknowledge the support by HPC Platform, Xi'an Jiaotong University.

Appendix A. Supplementary data

Supplementary data to this article can be found online at https://doi.org/10.1016/j.mtphys.2024.101549.

References

[1] L.E. Bell, Science 321 (2008) 1457.
[2] N. Li, J. Ren, L. Wang, G. Zhang, P. Hänggi, B. Li, Rev. Mod. Phys. 84 (2012) 1045.
[3] S.V. Garimella, A.S. Fleischer, J.Y. Murthy, A. Keshavarzi, R. Prasher, C. Patel, S. H. Bhavnani, R. Venkatasubramanian, R. Mahajan, Y. Joshi, B. Sammakia, B. A. Myers, L. Chorosinski, M. Baelmans, P. Sathyamurthy, P.E. Raad, IEEE Trans. Compon. Packag. Technol. 31 (2008) 801.
[4] R. Van Erp, R. Soleimanzadeh, L. Nela, G. Kampitsis, E. Matioli, Nature 585 (2020) 211.
[5] J. Liang, A. Kobayashi, Y. Shimizu, Y. Ohno, S.-W. Kim, K. Koyama, M. Kasu, Y. Nagai, N. Shigekawa, Adv.Mater 33 (2021): 2104564.
[6] C. Mion, J.F. Muth, E.A. Preble, D. Hanser, Appl. Phys. Lett. 89 (2006): 092123.
[7] G.J. Snyder, E.S. Toberer, Nat. Mater. 7 (2008) 105.
[8] J. He, T.M. Tritt, Science 357 (2017): eaak9997.
[9] Q.D. Gibson, T. Zhao, L.M. Daniels, H.C. Walker, R. Daou, S. Hébert, M. Zanella, M. S. Dyer, J.B. Claridge, B. Slater, M.W. Gaultois, F. Corà, J. Alaria, M.J. Rosseinsky, Science 373 (2021) 1017.
[10] L.-D. Zhao, S.-H. Lo, Y. Zhang, H. Sun, G. Tan, C. Uher, C. Wolverton, V.P. Dravid, M.G. Kanatzidis, Nature 508 (2014) 373.
[11] L. Lindsay, D.A. Broido, Phys. Rev. B 81 (2010): 205441.
[12] H. Bao, J. Chen, X. Gu, B. Cao, ES Energy Environ 1 (2018) 16.
[13] J.-S. Wang, J. Wang, N. Zeng, Phys. Rev. B 74 (2006): 033408.
[14] K.-Q. Chen, W.-X. Li, W. Duan, Z. Shuai, B.-L. Gu, Phys. Rev. B 72 (2005): 045422.
[15] P. Kim, L. Shi, A. Majumdar, P.L. McEuen, Phys. Rev. Lett. 87 (2001): 215502.
[16] D. Liu, R. Xie, N. Yang, B. Li, J.T. Thong, Nano Lett. 14 (2014) 806.
[17] A.A. Balandin, S. Ghosh, W. Bao, I. Calizo, D. Teweldebrhan, F. Miao, C.N. Lau, Nano Lett. 8 (2008) 902.
[18] D.G. Cahill, R.O. Pohl, Phys. Rev. B 35 (1987) 4067.
[19] Y. Hu, L. Zeng, A.J. Minnich, M.S. Dresselhaus, G. Chen, Nat. Nanotechnol. 10 (2015) 701.
[20] A.A. Balandin, Nat. Mater. 10 (2011) 569.
[21] P.-C. Wei, S. Bhattacharya, J. He, S. Neeleshwar, R. Podila, Y. Chen, A. Rao, Nature 539 (2016) E1.
[22] G.A. Slack, Solid State Phys. 34 (1979) 1.
[23] G. Qin, Y. Wei, L. Yu, J. Xu, J. Ojih, A.D. Rodriguez, H. Wang, Z. Qin, M. Hu, J. Mater. Chem. A 11 (2023) 5801.
[24] J. Ojih, C. Shen, A. Rodriguez, H. Zhang, K. Choudhary, M. Hu, J. Mater. Chem. A 11 (2023): 24169.
[25] J. Ojih, M. Al-Fahdi, Y. Yao, J. Hu, M. Hu, J. Mater. Chem. A 12 (2024) 8502.
[26] G. Qin, A. Huang, Y. Liu, H. Wang, Z. Qin, X. Jiang, J. Zhao, J. Hu, M. Hu, Mater. Adv. 3 (2022) 6826.

[27] J. Ojih, A. Rodriguez, J. Hu, M. Hu, Energy and AI 14 (2023): 100286.
[28] J. Callaway, Phys. Rev. 113 (1959) 1046.
[29] L. Chen, H. Tran, R. Batra, C. Kim, R. Ramprasad, Comput. Mater. Science 170 (2019): 109155.
[30] X. Wan, W. Feng, Y. Wang, H. Wang, X. Zhang, C. Deng, N. Yang, Nano Lett. 19 (2019) 3387.
[31] Y. Luo, M. Li, H. Yuan, H. Liu, Y. Fang, npj Comput. Mater. 9 (2023) 4.
[32] C. Loftis, K. Yuan, Y. Zhao, M. Hu, J. Hu, A J. Phys. Chem. A 125 (2020) 435.
[33] J. Liu, S. Han, G. Cao, Z. Zhou, C. Sheng, H. Liu, J. Phys. D Appl. Phys. 53 (2020): 315301.
[34] S. Curtarolo, W. Setyawan, G.L. Hart, M. Jahnatek, R.V. Chepulskii, R.H. Taylor, S. Wang, J. Xue, K. Yang, O. Levy, M.J. Mehl, H.T. Stokes, D.O. Demchenko, D. Morgan, Com. Mat, Science 58 (2012) 218.
[35] A. van Roekeghem, J. Carrete, C. Oses, S. Curtarolo, N. Mingo, Phys. Rev. X 6 (2016): 041061.
[36] Z. Gao, F. Tao, J. Ren, Nanoscale 10 (2018): 12997.
[37] X. Wang, Z. Gao, G. Zhu, J. Ren, L. Hu, J. Sun, X. Ding, Y. Xia, B. Li, Phys. Rev. B 107 (2023): 214308.
[38] D.T. Morelli, G.A. Slack, in: S.L. Shindé, J.S. Goela (Eds.), High Thermal Conductivity Materials, Springer New York, New York, NY, 2006, pp. 37–68.
[39] C.L. Julian, Phys. Rev. 137 (1965) A128.
[40] C. Toher, C. Oses, J.J. Plata, D. Hicks, F. Rose, O. Levy, M. de Jong, M. Asta, M. Fornari, M. Buongiorno Nardelli, S. Curtarolo, Phys. Rev. Mater. 1 (2017): 015401.
[41] T. Jia, G. Chen, Y. Zhang, Phys. Rev. B 95 (2017): 155206.
[42] L. Wei, P. Kuo, R. Thomas, T. Anthony, W. Banholzer, Phys. Rev. Lett. 70 (1993) 3764.
[43] M. Fujii, X. Zhang, H. Xie, H. Ago, K. Takahashi, T. Ikuta, H. Abe, T. Shimizu, Phy. Rev. Lett. 95 (2005): 065502.
[44] D. Morelli, J. Heremans, G. Slack, Phys. Rev. B 66 (2002): 195304.
[45] D.M. Teter, MRS Bull. 23 (1998) 22.
[46] X.-Q. Chen, H. Niu, D. Li, Y. Li, Intermetallics 19 (2011) 1275.
[47] P. Klemens, Solid State Phys. 7 (1958) 1.
[48] N. Surplice, R. Jones, Br. J. Appl. Phys. 14 (1963) 720.
[49] C. Herring, Phys. Rev. 95 (1954) 954.
[50] J.D. Beasley, Appl. Opt. 33 (1994) 1000.
[51] G.A. Slack, Phys. Rev. 126 (1962) 427.
[52] L. Bjerg, B.B. Iversen, G.K.H. Madsen, Phys. Rev. B 89 (2014): 024304.
[53] E.S. Toberer, A. Zevalkink, G.J. Snyder, J. Mater. Chem. 21 (2011): 15843.
[54] G.A. Slack, J. Appl. Phys. 35 (12) (1964) 3460–3466.
[55] M. Feng, X. Wang, G. Zhu, C. He, J. Sun, X. Ding, J. Shiomi, Y. Xia, B. Li, Z. Gao, Mater. Today. Phys. 44 (2024): 101423.
[56] X. Qian, J. Zhou, G. Chen, Nat. Mater. 20 (2021) 1188.
[57] T. Xie, J.C. Grossman, Phys. Rev. Lett. 120 (2018): 145301.
[58] T. Tadano, S. Tsuneyuki, Phys. Rev. B 92 (2015): 054301.
[59] Y. Xia, V.I. Hegde, K. Pal, X. Hua, D. Gaines, S. Patel, J. He, M. Aykol, C. Wolverton, Phys. Rev. X 10 (2020): 041029.
[60] Y. Xiao, L.-D. Zhao, Science 367 (2020) 1196.
[61] J. He, M. Amsler, Y. Xia, S.S. Naghavi, V.I. Hegde, S. Hao, S. Goedecker, V. Ozoliņš, C. Wolverton, Phys. Rev. Lett. 117 (2016): 046602.
[62] K. Kuroki, R. Arita, J. Phys. Soc. Jpn. 76 (2007): 083707.
[63] H. Liu, X. Shi, F. Xu, L. Zhang, W. Zhang, L. Chen, Q. Li, C. Uher, T. Day, G. J. Snyder, Nat. Mater. 11 (2012) 422.